



## Severe sink-in occurrence in thermally sprayed hydroxyapatite coating

Saeed Saber-Samandari<sup>1,\*</sup>, Saeid Baradaran<sup>1</sup>, Bahman Nasiri-Tabrizi<sup>1</sup>, Kadhim Alamara<sup>2</sup>, Wan Jeffrey Basirun<sup>3</sup>

<sup>1</sup>New Technologies Research Center, Amirkabir University of Technology, Tehran, Iran

<sup>2</sup>Sustainable and Renewable Energy Engineering (SREE), University of Sharjah, United Arab Emirates

<sup>3</sup>Department of Chemistry, Faculty of Science, University of Malaya, 50603 Kuala Lumpur, Malaysia

Received 6 March 2018; Received in revised form 11 June 2018; Accepted 22 June 2018

### Abstract

The performance of orthopaedic and dental implants counts on the ability to appraise the mechanical properties of biomaterials. In the present study, nanoindentation was used to characterize the mechanical properties of thermally sprayed hydroxyapatite-coated commercial pure titanium (HA/CP-Ti). From the XRD patterns, the as-sprayed HA coating showed an inhomogeneous mixture of polycrystalline and amorphous phases along with the formation of the decomposed constituents including tricalcium phosphate ( $\alpha$ -TCP), tetracalcium phosphate (TTCP) and calcium oxide (CaO). The SEM micrographs of HA coating indicated some incompletely melted particles on the surface of flattened droplets, where the average pore size was around 0.8  $\mu\text{m}$ . After the load-unload indentation experiment, a clear severe sink-in deformation feature was observed around the residual indentation impression of the amorphous part. In contrast, pile-up only occurs during loading for the crystalline part of the coating. In addition, the crystalline part of the coating exhibited a Young's modulus and hardness of around 120.46 and 7.91 GPa, respectively, which were almost 8 and 259% higher than that of the bare CP-Ti substrate. This is the first report on the nanoindentation characterization of the inhomogeneous mixture of various phase structures in thermally sprayed HA coatings.

**Keywords:** thermal spraying, hydroxyapatite coating, nanoindentation, mechanical behaviour, severe sink-in

### I. Introduction

Among various metallic biomaterials, titanium (Ti) and Ti-based alloys are widely employed for dental and orthopaedic implants due to their excellent corrosion resistance and mechanical properties. However, this type of biomaterial cannot meet all of the clinical requirements and thus surface-modification techniques may be used to decrease wear and corrosion, which may occur at the implant level [1,2]. To improve the bone-implant coupling and the therapeutic process, the incorporation of calcium phosphate coatings is constantly being reviewed [3–6]. Among them, hydroxyapatite (HA) coatings are utilized in clinical applications, especially for coating of metallic implants because of their chemical similarity to the mineral constituent of natural bone as well as excellent biocompatibility, bioactivity and

biodegradability [7–11]. For successful performance of the main functions, bioceramic coatings should meet numerous obligations. Therefore, careful consideration should be given to the mechanical properties and long-term stability of the HA coatings [12].

Given that almost all kinds of materials can be developed on different substrates, many possibilities are accessible to categorize the accessible kinds of coatings. For instance, they might be sorted in accordance with the development method, where all kinds of coatings can be grouped into two big classes including conversion ones, which are generated by reaction products of the base material and deposited ones [13]. Further, the deposited approach might be categorized in accordance with the deposition methods, such as plasma spraying, high-velocity oxy-fuel spraying, RF magnetron sputtering, pulsed laser deposition (laser ablation), dip coating, ion beam assisted deposition, electrostatic spray deposition, spin coating, sol-gel technique, electrophoretic deposition, electrochemical (cathodic) deposition, biomimetic process, hydrothermal deposi-

\*Corresponding author: tel: +98 21 6454 5193,  
fax: +98 21 6640 2044,  
e-mail: [saeedss@aut.ac.ir](mailto:saeedss@aut.ac.ir) (S. Saber-Samandari)  
e-mail: [saeid\\_baradaran@aut.ac.ir](mailto:saeid_baradaran@aut.ac.ir) (S. Baradaran)

tion, thermal substrate deposition, hot isostatic pressing, micro-arc oxidation, and dynamic mixing method [14–18]. Among them, thermally sprayed HA coatings are widely used for various biomedical applications because of its ability to form thin HA coatings on a variety of orthopaedic prosthesis and dental implants [19–23]. Based on the literature, by choosing the optimum relation between particle sizes, type and pressure of gas, plasma rate and cooling cycle of the substrates, various coatings with tailored properties can be obtained. However, in view of the fact that thermal spraying takes place at very high temperatures, the formed hot droplets continuously heat up the undercoats, which might give rise to phase transition and recrystallization of the areas close to the surface. Indeed, such microstructural changes make further vagueness of the adhesive behaviour and mechanical properties of the coatings [13,24]. Accordingly, there is a necessity to assess the mechanical behaviour of the thermally sprayed HA-coated implant. In this regard, nanoindentation is more perceptive than that of the conventional analysis that just provides a quantitative assessment of the bonding within the coating. If necessary, nanoindentation could also be utilized in association with mechanical property distributions determined from indentation on the cross-section [23,25]. Therefore, the aim of the present work is to quantitatively assess the mechanical properties of HA/CP-Ti by nanoindentation test, where some unusual phenomena were also found around the residual indentation impression.

The impact of thermal spray parameters, such as preheating temperature, spray distance, feedstock morphology and particles size, angle of spraying, and particle velocity on mechanical properties of HA-coated implant are available in literature [26–28]. The coatings in the present work possess amorphous phases along with decomposed constituent [29]. Up to now, no research has comprehensively documented the effectiveness of the inhomogeneous mixture of various compounds on the nanoindentation properties of the thermally sprayed HA coatings. Thus, this work more specifically addresses the effect of phase constituents (i.e. polycrystalline and amorphous phases) on mechanical properties including hardness and elastic modulus of HA coating.

## II. Materials and methods

### 2.1. Preparation of HA coating

The CP-Ti substrate was prepared by grinding SiC abrasive paper of 320 grit size at a speed of 300 rpm for 1 min. After that, fine grinding was performed on an MD-Largo surface for 4 min with DiaPro Allegro (Struers) as the lubricant for faster, more cost-efficient and much easier materialographic sample preparation. The final polishing was then conducted using 0.04  $\mu\text{m}$  colloidal silica on a MD-Chem cloth for 5 min. Prior to thermal spray coating, HA powder (CAM implants, Netherlands) was sieved to a particle size of 20–40  $\mu\text{m}$ .

The sieved powder was passed through into a powder feeder (Metco 3MP, Sulzer Metco, Wohlen, Switzerland) and then into a flame spray torch (Metco 5P, Sulzer Metco, Wohlen, Switzerland) operated with acetylene and oxygen, with air as the carrier gas at a flow rate of 50 g/min. The acetylene and oxygen pressures were 103 and 200 kPa, respectively. The polished CP-Ti substrate was placed 15 cm from the torch and the HA powder was sprayed onto the 300 °C preheated substrate surface. Half of the treated specimen was mounted in epoxy resin (Aka-Resin & Aka-Cure, Denmark) to make support throughout the cross-sectional cutting and metallographic preparation to obtain smooth sample surfaces for the nanoindentation experiments. Fine grinding was performed with SiC abrasive papers of decreasing grit size (800, 1200 and 2400 grit) and polishing included a 3 micron diamond suspension on a Largo surface followed by a 0.05  $\mu\text{m}$  colloidal silica on an OPS cloth. Hereon, the spraying parameters were regulated to attain maximum coating constancy and homogeneity on the basis of literature and previous pilot studies [30–32]. Figure 1 shows a schematic illustration of the thermal spraying process used in the present research.

### 2.2. Coating characterization

The phase compositions of feedstock powder and HA coating were determined using an X-ray diffractometer (Philips PW1800) with Cu-K $\alpha$  radiation at 40 kV and 30 mA over a  $2\theta$  range between 10° and 80° with the step size of 0.02° and a fine slit. The surface morphology of the as-sprayed coatings was examined with a scanning electron microscopy (XL30 Philips). Energy-

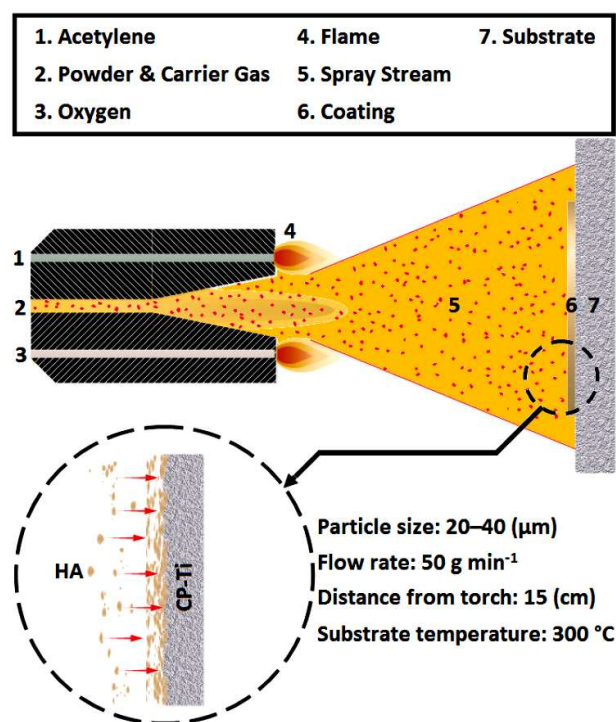


Figure 1. Schematic illustration of the thermal spraying process used in the present research

dispersive X-ray spectrometry (EDS) outfitted with the SEM was used to determine the chemical composition of the specimens. The surface roughness parameters,  $R_a$  (arithmetic average) and  $R_t$  (maximum height of the profile) were measured using an XP-2 High Resolution Surface Profilometer, Ambios Technology, Inc., CA, USA. Mechanical properties of the HA coatings were determined by a nano-based indentation system (Ultra Micro-Indentation System, UMIS-2000, CSIRO, Australia) with a calibrated Berkovich indenter (three-sided pyramidal) (Synton, Switzerland). Herein, a series of indentations were made on the cross-sectional surfaces of the samples using a peak load of 50 mN, where UMIS software based on the Oliver-Pharr method was employed to determine Young's modulus ( $E$ ) and hardness ( $H$ ). It is necessary to mention that all nanoindentation experiments commenced after a thermal soak of the instrument, minimum for 1 h, so the thermal drift was deemed to be almost negligible ( $<0.05 \text{ nm s}^{-1}$ ) before each test.

### III. Results and discussion

#### 3.1. Phase analysis

Figure 2 shows the XRD patterns of a reference amorphous calcium phosphate (ACP) coating, the feedstock HA powder and thermally sprayed HA coating. From Fig. 2a, a broad peak assigned to an amorphous phase is observed in the XRD profile of the stress-relieved ACP [33]. On the other hand, the crystalline structure in the feedstock HA powder demonstrates well-defined peaks in the X-ray diffraction pattern, where the typical lattice

fringes with  $d$  parameters of 0.344, 0.281, 0.277, 0.272, 0.263, 0.226, 0.194, 0.184, and 0.172 nm are ascribed to (002), (211), (112), (300), (202), (310), (222), (213), and (004) planes of HA (JCPDS #09-0432), respectively (Fig. 2b).

As shown in Fig. 2c, the diffraction profile of the as-sprayed HA coating demonstrates broad peaks at  $31.7^\circ$ ,  $49.4^\circ$ , and  $53.1^\circ$ . This suggests that the as-deposited HA coating possesses an inhomogeneous mixture of polycrystalline and amorphous phases along with the formation of the decomposed constituents including two main diffraction peaks corresponding to (200) and (040) planes of TTCP (#025-1137) with monoclinic structure, the (170) crystal plane of  $\alpha$ -TCP (#09-0348) with orthorhombic structure and a minor peak attributed to (200) plane of CaO (#037-1497). The lattice constants ( $a$ - and  $c$ -axis) and unit cell volume ( $V$ ) of the as-sprayed HA coating are illustrated in Fig. 2d,e,f. Based on the obtained data, the lattice parameters of the standard HA (JCPDS #09-0432) along the  $a$ - and  $c$ -axis are 9.418 and 6.884 Å, respectively, whereas these values decreased to 9.404 and 6.881 Å for the as-sprayed HA coating (Fig. 2d,e). Accordingly, the unit cell volume decreased from  $528.8 \text{ \AA}^3$  for the standard to  $527.0 \text{ \AA}^3$  for the as-sprayed HA coating, which is consistent with XRD peaks shifting toward higher angles (Fig. 2f). In this case, a dramatic decrease in the cell volume could be attributed to the substitution of  $\text{PO}_4^{3-}$  with  $\text{CO}_3^{2-}$  groups in the HA lattice owing to the smaller ionic radius of the carbonate (1.78 Å) than of the phosphate (2.38 Å) [34]. To appraise the lattice mismatch, the in-plane ( $\varepsilon_a$ ) and out-of-plane ( $\varepsilon_c$ ) strains were measured

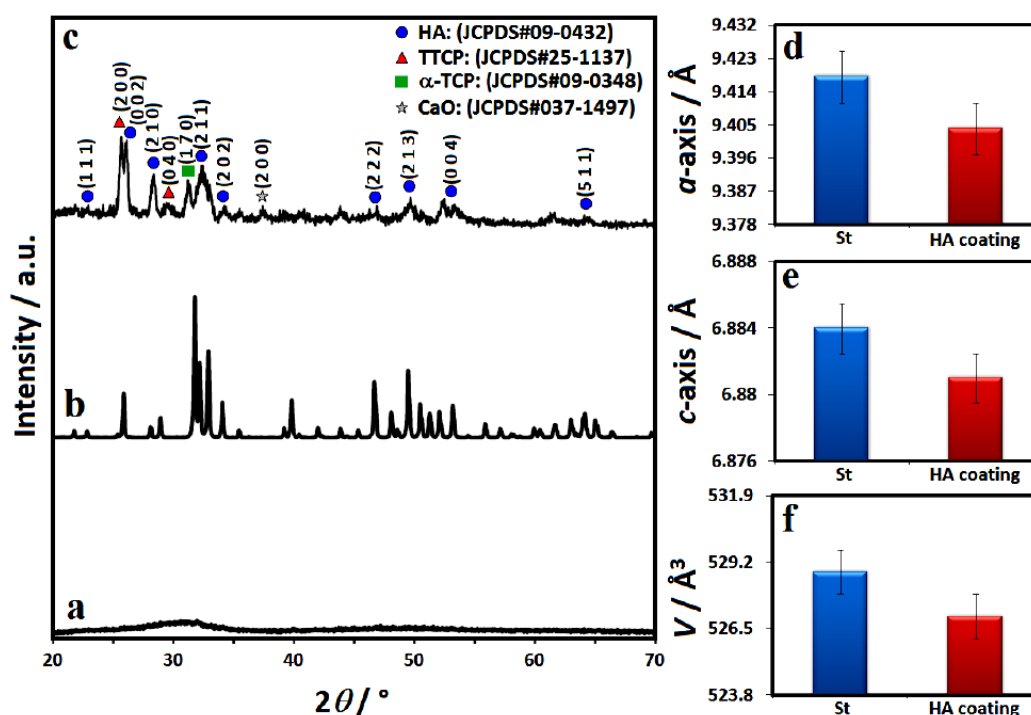
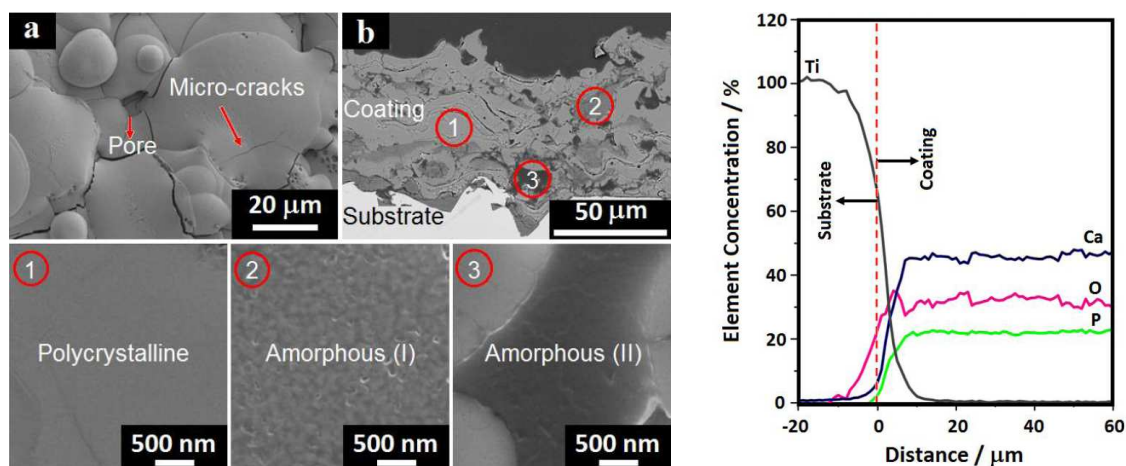


Figure 2. XRD patterns of: a) a reference ACP coating, b) the feedstock HA powder [33] and c) thermally sprayed HA coating, as well as the  $a$ - and  $c$ -lattice constants (d,e) and unit cell volume,  $V$  (f) of the HA coating



**Figure 3.** Typical top- (a) and cross-sectional (b) SEM micrographs, as well as the EDS line scan analysis (c) of the as-sprayed HA coating on CP-Ti substrate

by contrasting the lattice parameters of the HA coating with the lattice parameters of unstrained HA [35]:

$$\varepsilon_a = \frac{a - a_0}{a_0} \quad (1)$$

$$\varepsilon_c = \frac{c - c_0}{c_0} \quad (2)$$

The in-plane and out-of-plane strains of the as-sprayed HA coating are  $-0.001$  and  $-0.0004$ , respectively, where the negative values of the strains point out the compressive strain in the coating. This result shows that there is just minor lattice disparity as the  $\text{PO}_4^{3-}$  groups are replaced by the  $\text{CO}_3^{2-}$ .

### 3.2. Surface properties and EDS analysis

Figure 3 shows the typical top- and cross-sectional SEM micrographs as well as the EDS line scan analysis of the as-sprayed HA coating on CP-Ti substrate. SEM image (Fig. 3a) confirms that the as-sprayed HA coating exhibits some partly melted particles on the surface of flattened droplets.

Similar observations were also reported in previous study [13]. It is found that dimensions of the feedstock HA powder can affect the melting characteristics within the thermal spraying process, where coarser particles undergo a lesser degree of melting compared to smaller particles. For instance, HA particles with sizes above  $\sim 55 \mu\text{m}$  were observed to stay crystalline and demonstrated slight or no melting throughout thermal spraying. On the other hand, while HA particles with sizes ranging between  $30\text{--}55 \mu\text{m}$  were partly melted and comprised of combinations of amorphous and crystalline phases. In addition, HA particles less than  $\sim 30 \mu\text{m}$  were completely melted and consisted of a large fraction of ACP and small amount of CaO [36].

From Fig. 3a, some micro-cracks and open pores with the average size of around  $0.8 \mu\text{m}$  are developed on the surface of the splats. Here, a residual tensile stress is unavoidable within the splats owing to the lower coefficient of thermal expansion of the CP-Ti ( $8.6 \times 10^{-6} \text{K}^{-1}$ )

than HA ( $16.0 \times 10^{-6} \text{K}^{-1}$ ), which would impact on the crack formation within the splat during the final step of solidification. On the other hand, among the decomposed components, the presence of high amounts of CaO in the coating makes adverse effects because hydration reactions happening throughout storage or after implantation transform calcium oxide into calcium hydroxide with  $\sim 50\%$  volume increasing, causing significant internal strains and cracks [13]. Moreover, the small micro-pores are generated due to the isolated pores within the feedstock HA powder. These small gas bubbles would coalesce to form a large bubble within the droplet in accordance with the dynamics of gas bubble within liquid [37].

The cross-sectional SEM micrograph of the HA coating in Fig. 3b shows good bonding between the ceramic coating and metallic substrate. From this figure, the as-sprayed HA coating exhibits an average thickness of  $70 \pm 4 \mu\text{m}$ , measured at 5 positions on a polished cross-section and then averaged. Due to the inherent brittleness of the HA material, the microcracks were formed during the polishing procedure. From the cross-sectional SEM image in Fig. 3b, the spreading of amorphous phases and by-products is inhomogeneous. This structure contains three domains with different contrast, including i) light grey, ii) grey and iii) dark, which represent polycrystalline phase, amorphous phase (I) and amorphous phase (II), respectively. The formation of these various admixtures and metastable phases is due to the very high processing temperature, which results in incongruent melting together with an incomplete dehydroxylation of HA, and a negligible decomposition of other phases, followed by a fast solidification [13]. This is consistent with the XRD profiles, indicating that an inhomogeneous mixture of polycrystalline and amorphous phases is formed during thermal spraying of HA on the preheated CP-Ti substrate. The existence of such inhomogeneous structure can provide different properties than the initial bulk materials [38]. It is reported that the impact of the metastable and amorphous phases presence on the coating features depends on their posi-

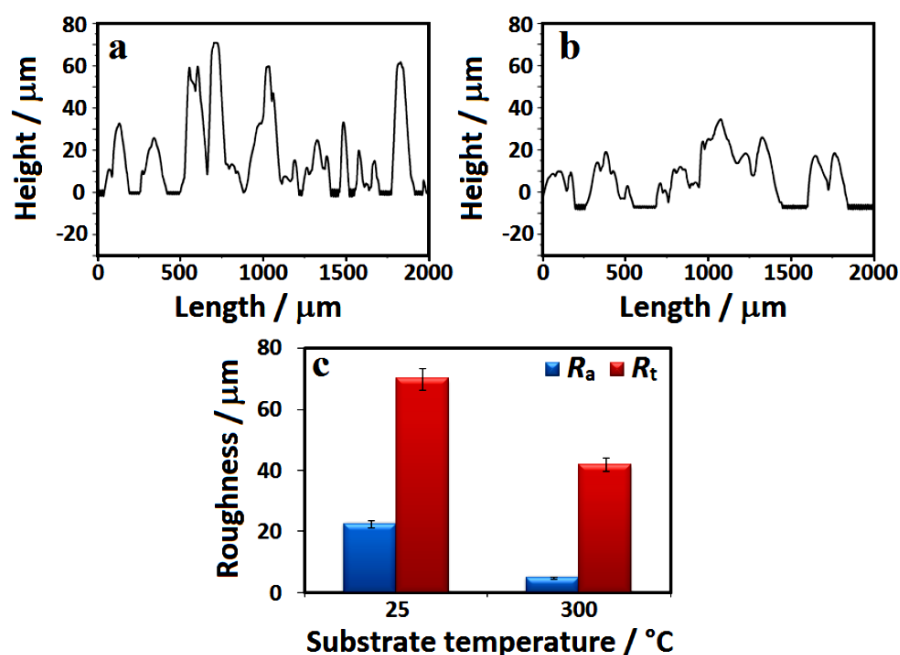


Figure 4. Surface roughness profiles for the as-sprayed HA coatings on the untreated (a) and preheated CP-Ti substrate (b) as well as surface roughness parameters,  $R_a$  and  $R_t$  (c)

tion. For instance, being positioned in the surface layer, such phases endorse growth of bone tissues because of a higher bioresorption, whereas close to the interface of coating-substrate, a rapid dissolution of these phases results in the adhesive strength falling and peeling off the deposits prior to the bone tissue generation [13].

From the EDS line scan analysis in Fig. 3c, the oxygen content is uniform throughout the thickness direction from the coating surface to the Ti–HA interface, which is consistent with the desired HA composition. On the contrary, Ca and P contents slowly reduce at 7  $\mu\text{m}$  from the interface. This suggests that the presence of O is vital to the development of the HA coating. It is important to stress that the presence of Ti in the deposit verifies its diffusion within the coating owing to the preheating of the CP-Ti substrate before the coating process.

In general, the roughness of coating might be applied as a measure of the particles melting degree. For example, as the deposited particles reach a more fluid state during the plasma flame they turn into less viscous. Accordingly, they can be expanded to a greater degree over the undercoat, where a smoother layer is formed. On the other hand, partly melted particles cannot squash simply on the surface, leading to large fluctuations and rough coatings [39]. Figure 4 displays the surface roughness profiles for the as-sprayed HA coatings on the untreated and preheated CP-Ti substrate as well as surface roughness parameters ( $R_a$  and  $R_t$ ).

As can be seen in Fig. 4, the HA coating on preheated substrate possesses lower roughness compared to the untreated sample. This behaviour can be caused by the enhanced spreading of melted particles over the surface [13]. The results of surface roughness measurements for the HA coatings showed that the  $R_a$  and  $R_t$  values for the

untreated sample are  $22.5 \pm 1.1$  and  $70.0 \pm 3.3$   $\mu\text{m}$ , respectively (Fig. 4c). These values reached  $5.0 \pm 0.2$  and  $42.0 \pm 2.1$   $\mu\text{m}$  in the case of preheated CP-Ti substrate, which is consistent with the previous findings that deposits with surface roughness values of  $R_a = 7, 10$  and  $24$   $\mu\text{m}$  were produced by thermal spraying [39].

### 3.3. Nanoindentation assessment

Figure 5 shows schematic views of the deformed surfaces after tip removal, load-displacement curves and residual impressions of indentation for elastic, plastic and elastic-plastic indentations. The sense of loading and unloading is shown by the arrows. In the case

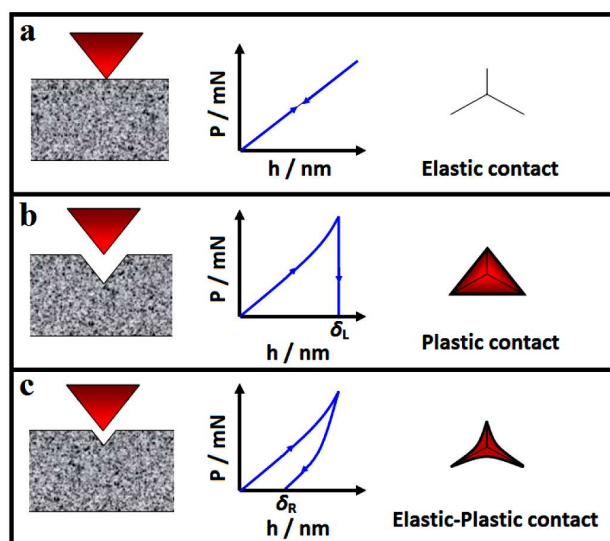
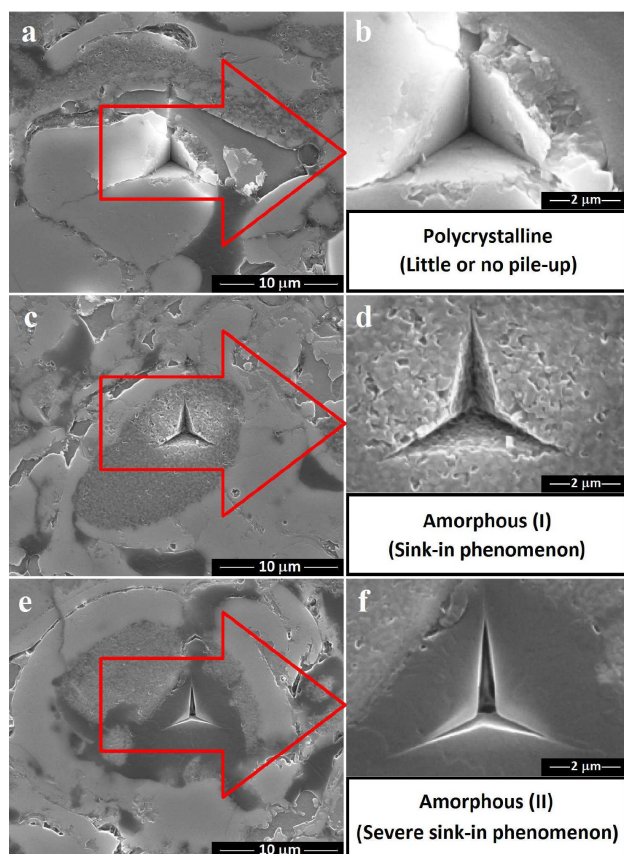


Figure 5. Schematic views of the deformed surfaces after tip removal, load-displacement curves and residual impressions of indentation for: a) elastic, b) plastic and c) elastic-plastic indentations



**Figure 6.** SEM micrographs of nanoindentations created with a Berkovich indenter in a cross-section of HA/CP-Ti; polycrystalline phase (a,b), amorphous phase (I) (c,d) and amorphous phase (II) (e,f)

of fully elastic contact, the proportion of the loaded displacement recoverable during unloading is 100%. Therefore, no impression of the indentation is observed after unloading as shown in Fig. 5a. In contrast, the proportion of the loaded displacement recoverable during unloading for fully plastic contact response is 0%, where the maximum total surface deflection ( $\delta_L$ ) is recorded for a given applied load  $P$  (Fig. 5b). In this case, no deformation takes place until yield stress is attained as plastic flow occurs. Besides, no recovery during unloading is detected and the impression remains unchanged. Typical load-displacement curve for elastic-plastic behaviour is also presented in Fig. 5c, where  $\delta_R$  is the recorded displacement following elastic recovery of the surface flexure, which presents a measurement of the plastic component of the surface response [40,41]. Nanoindentation has the ability to be used as a probing tool to characterize the alteration in mechanical behaviour through the coating thickness. The SEM micrographs of nanoindentations created with a same indenter (Berkovich indenter) in a cross-section of HA/CP-Ti are shown in Fig. 6.

The SEM images in Figs. 6a and 6b reveal the presence of microcracks and deformations around the indenter. In addition, the HA coating shows little or no pile-up at the edges of the indenter in the crystalline part of the coating. A deep penetration of the indenter in the

crystalline part of the coating can be caused by being in the vicinity of the amorphous phase and the presence of cracks [12]. From Figs. 6c and 6d, near the contact zone, one can see that the amorphous phase (I) region of the HA coating is downwards against the tip of indenter which makes a sink-in on the rims. In the amorphous phase (II) region, severe sink-in is observed which confirms that this region of the HA coating has higher strain-hardening ability than the other parts as the surface surrounding the indenter has a great tendency to sink-in (Figs. 6e and 6f). A similar behaviour was observed by Mullins *et al.* [42] for cortical bone during nanoindentation, but they have not described this phenomenon.

In general, pile-up and sink-in are the most important phenomena during nanoindentation tests, which show the deformation of specimen around the contact point. These phenomena are connected to the nanoindentation of elastic-plastic materials. In the pile-up phenomenon, contact depth is always deeper than the total depth of indentation, accordingly the projected area is always underestimated. This underestimated area could overestimate both hardness and reduced elastic modulus, with a more noteworthy impact on hardness [32]. In contrast, the sink-in leads to contact area that is smaller than the cross-sectional area. As these phenomena can drastically affect the contact area and can cause imprecise calculations of the indented material, these deformations have large impacts on the measurements of indentation moduli. From the literature, highest pile-up is commonly diagnosed on the supposition of elastic-plastic materials, whereas highest sink-in takes place for strain-hardening materials. It is found that different materials can be deformed in different modes in the nearness of the contact point [43]. Consequently, it can be deduced that the observed deformations in different regions of the HA coating are related only to intrinsic material properties and cannot be derived from the applied load. Figure 7 shows the load-displacement curves for indentations into polycrystalline, amorphous (I) and (II)

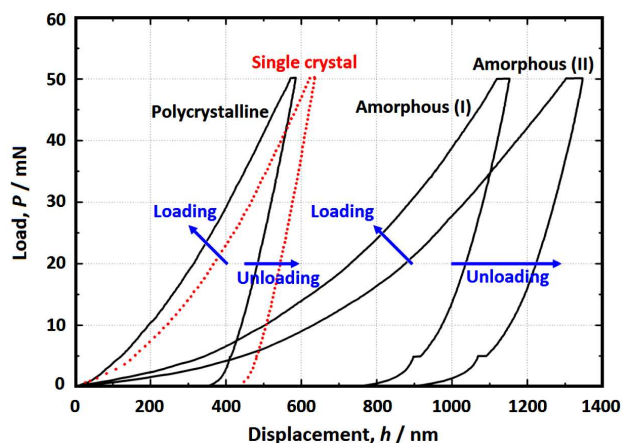


**Figure 7.** The load-displacement curves for indentations into polycrystalline, amorphous (I) and (II) regions of the HA coating compared to single crystal HA

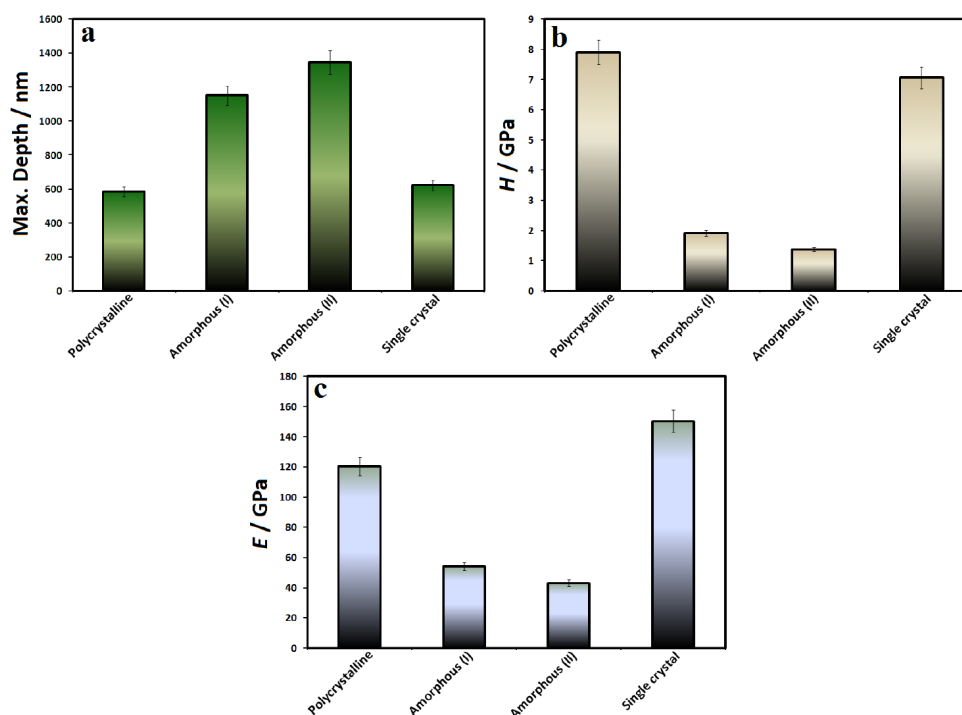


**Figure 8.** Maximum depth (a), hardness (b) and Young's modulus (c) values of the polycrystalline, amorphous (I) and (II) regions of the HA coating contrasted to the single crystal HA

regions of the HA coating compared to single crystal HA. In addition, maximum depth, hardness and Young's modulus values of the polycrystalline, amorphous (I) and (II) regions of the HA coating contrasted to the single crystal HA are shown in Fig. 8. It is obvious that the amorphous phases are effortlessly deformed as exposed in the horizontal displacement at the peak load. This shows that more creep occurs in the amorphous (I) and (II) regions compared to the crystalline phase [12].

As can be seen, the polycrystalline region of the HA coating is more resistant to indent and possesses higher hardness (7.91 GPa) and lower penetration depth (585 nm) than that of the single crystal HA (Figs. 8a and 8b). A dramatic decrease in the hardness value to 1.92 and 1.38 GPa is observed for the regions of the amorphous phases (I) and (II), respectively. The same trend is also seen in Young's modulus as shown in Fig. 8c, where the  $E$  values decreased from 120.46 GPa in the polycrystalline region to 54.28 and 43.02 GPa for the amorphous phases (I) and (II), respectively. This feature can be linked to the random distribution of defects within the thermally sprayed coatings as one of the key factors responsible for the anisotropy in mechanical properties of the coating [37].

#### IV. Conclusions

A new approach on the nanoindentation characterization of the inhomogeneous mixture of various phase structures in thermally sprayed HA coatings was developed. The XRD results showed that the as-deposited HA coating contained an inhomogeneous mixture of polycrystalline and amorphous phases along with the forma-

tion of the decomposed constituents. From the structural assessment, the unit cell volume declined to  $527.0 \text{ \AA}^3$  for the as-sprayed HA coating. Besides, the in-plane and out-of-plane strains of the as-sprayed HA coating exhibited a minor lattice disparity compared to standard HA. From the SEM observations, the as-sprayed HA coating had a mean thickness of  $70 \pm 4 \mu\text{m}$ , where the distribution of by-products and amorphous phases was inhomogeneous. The observed deformations in different regions of the HA coating were related only to intrinsic material properties, where severe sink-in was detected in the amorphous phase (II) region. Based on the nanoindentation behaviour, the polycrystalline region of the HA coating was more resistant to indent and showed the highest hardness of 7.91 GPa and lowest penetration depth of 585 nm. In addition, a significant decrease in the hardness value was observed for the regions of the amorphous phases. A same trend was also noticed in Young's modulus. It can be concluded that the random distribution of defects within inhomogeneous phase states had significant effects on the anisotropy in mechanical behaviour of the thermally sprayed HA coatings.

**Acknowledgement:** The authors would like to acknowledge the Amirkabir University of Technology for providing necessary resources and facilities for the present study.

#### References

1. M. Sarraf, B.A. Razak, R. Crum, C. Gámez, B. Ramirez, N.H.B. Abu Kasim, B. Nasiri-Tabrizi, V. Gupta, N.L.

- Sukiman, W.J. Basirun, “Adhesion measurement of highly-ordered TiO<sub>2</sub> nanotubes on Ti-6Al-4V alloy”, *Process. Appl. Ceram.*, **11** [4] (2017) 311–321.
2. A. Rafieerad, A. Bushroa, B. Nasiri-Tabrizi, A. Fallahpour, J. Vadivelu, S. Musa, S. Kaboli, “GEP-based method to formulate adhesion strength and hardness of Nb PVD coated on Ti6Al4Nb aimed at developing mixed oxide nanotubular arrays”, *J. Mech. Behav. Biomed. Mater.*, **61** [9] (2016) 182–196.
  3. T. Mokabber, L.Q. Lu, P. van Rijn, A.I. Vakis, Y.T. Pei, “Crystal growth mechanism of calcium phosphate coatings on titanium by electrochemical deposition”, *Surf. Coat. Technol.*, **334** [2] (2018) 526–535.
  4. S. Bose, D. Banerjee, A. Shivaram, S. Tarafder, A. Bandyopadhyay, “Calcium phosphate coated 3D printed porous titanium with nanoscale surface modification for orthopedic and dental applications”, *Mater. Des.*, **151** [15] (2018) 102–112.
  5. A.M. Vilardeell, N. Cinca, I.G. Cano, A. Concustell, S. Dosta, J.M. Guilemany, S. Estradé, A. Ruiz-Caridad, F. Peiró, “Dense nanostructured calcium phosphate coating on titanium by cold spray”, *J. Eur. Ceram. Soc.*, **37** [4] (2017) 1747–1755.
  6. G. Graziani, M. Bianchi, E. Sassoni, A. Russo, M. Maracci, “Ion-substituted calcium phosphate coatings deposited by plasma-assisted techniques: A review”, *Mater. Sci. Eng. C*, **74** [6] (2017) 219–229.
  7. K. Dudek, M. Dulski, T. Goryczka, A. Gerle, “Structural changes of hydroxyapatite coating electrophoretically deposited on NiTi shape memory alloy”, *Ceram. Int.*, **44** [10] (2018) 11292–11300.
  8. B. Zheng, Y. Luo, H. Liao, C. Zhang, “Investigation of the crystallinity of suspension plasma sprayed hydroxyapatite coatings”, *J. Eur. Ceram. Soc.*, **37** [15] (2017) 5017–5021.
  9. S. Bose, A.A. Vu, K. Emshadi, A. Bandyopadhyay, “Effects of polycaprolactone on alendronate drug release from Mg-doped hydroxyapatite coating on titanium”, *Mater. Sci. Eng. C*, **88** [7] (2018) 166–171.
  10. A. Karthika, “Alivalent ions substituted hydroxyapatite coating on titanium for improved medical applications”, *Mater. Today*, **5** [2] (2018) 8768–8774.
  11. C. Hu, L. Yu, M. Wei, “Sectioning studies of biomimetic collagen-hydroxyapatite coatings on Ti-6Al-4V substrates using focused ion beam”, *Appl. Surf. Sci.*, **444** [20] (2018) 590–597.
  12. K.A. Gross, S. Saber-Samandari, K.S. Heemann, “Evaluation of commercial implants with nanoindentation defines future development needs for hydroxyapatite coatings”, *J. Biomed. Mater. Res.*, **93B** [1] (2010) 1–8.
  13. S.V. Dorozhkin, “Calcium orthophosphate deposits: Preparation, properties and biomedical applications”, *Mater. Sci. Eng. C*, **55** [10] (2015) 272–326.
  14. Y. Yang, K.H. Kim, J.L. Ong, “A review on calcium phosphate coatings produced using a sputtering process - an alternative to plasma spraying”, *Biomaterials*, **26** [3] (2005) 327–337.
  15. R. Narayanan, S.K. Seshadri, T.Y. Kwon, K.H. Kim, “Calcium phosphate-based coatings on titanium and its alloys”, *J. Biomed. Mater. Res.*, **85B** [1] (2008) 279–299.
  16. A.R. Rafieerad, A.R. Bushroa, B. Nasiri-Tabrizi, S. Baradaran, S. Shahtalebi, S. Khanahmadi, M. Afshar-Mohajer, J. Vadivelu, F. Yusof, W.J. Basirun, “In-vitro bioassay of electrophoretically deposited hydroxyapatite-zirconia nanocomposite coating on Ti-6Al-7Nb implant”, *Adv. Appl. Ceram.*, **116** [6] (2017) 293–306.
  17. R. Narayanan, K.H. Kim, T.R. Rautray, *Surface Modification of Titanium for Biomaterial Applications*, Nova Science, Hauppauge, NY, USA, 2010. (352 pp.).
  18. A.R. Rafieerad, M.R. Ashra, R. Mahmoodian, A.R. Bushroa, “Surface characterization and corrosion behavior of calcium phosphate-base composite layer on titanium and its alloys via plasma electrolytic oxidation: A review paper”, *Mater. Sci. Eng. C*, **57** [12] (2015) 397–413.
  19. M. Aoyagi, M. Hayashi, Y. Yoshida, Y. Yao, *Implants for Bones Joints and Tooth Roots*, US Patent No. 4146936, 1979.
  20. R. Gadow, A. Killinger, N. Stiegler, “Hydroxyapatite coatings for biomedical applications deposited by different thermal spray techniques”, *Surf. Coat. Technol.*, **205** [4] (2010) 1157–1164.
  21. K.A. Gross, S. Saber-Samandari, “Revealing mechanical properties of a suspension plasma sprayed coating with nanoindentation”, *Surf. Coat. Technol.*, **203** [20-21] (2009) 2995–2999.
  22. S. Saber-Samandari, K.A. Gross, “The use of thermal printing to control the properties of calcium phosphate deposits”, *Biomaterials*, **31** [25] (2010) 6386–6393.
  23. S. Saber-Samandari, K.A. Gross, “Nanoindentation reveals mechanical properties within thermally sprayed hydroxyapatite coatings”, *Surf. Coat. Technol.*, **203** [12] (2009) 1660–1664.
  24. G.L. Zhao, G. Wen, Y. Song, K. Wu, “Near surface martensitic transformation and recrystallization in a Ti-24Nb-4Zr-79Sn alloy substrate after application of a HA coating by plasma spraying”, *Mater. Sci. Eng. C*, **31** [2] (2011) 106–113.
  25. S. Saber-Samandari, K.A. Gross, “Nanoindentation on the surface of thermally sprayed coatings”, *Surf. Coat. Technol.*, **203** [23] (2009) 3516–3520.
  26. A.J. Wang, Y.P. Lu, C.Z. Chen, R.X. Sun, “Effect of plasma spraying parameters on the sprayed hydroxyapatite coating”, *Surf. Rev. Lett.*, **14** [2] (2007) 179–184.
  27. S.W.K. Kweh, K.A. Khor, P. Cheang, “Plasma-sprayed hydroxyapatite (HA) coatings with flame-spheroidized feedstock: microstructure and mechanical properties”, *Biomaterials*, **21** [12] (2000) 1223–1234.
  28. S. Dyshlovenko, L. Pawlowski, P. Roussel, D. Murano, A. Le Maguer, “Relationship between plasma spray operational parameters and microstructure of hydroxyapatite coatings and powder particles sprayed into water”, *Surf. Coat. Technol.*, **200** [12-13] (2006) 3845–3855.
  29. K.A. Gross, V. Gross, C.C. Berndt, “Thermal analysis of amorphous phases in hydroxyapatite coatings”, *J. Am. Ceram. Soc.*, **81** [1] (1998) 106–112.
  30. S. Saber-Samandari, K. Alamara, S. Saber-Samandari, K.A. Gross, “Micro-Raman spectroscopy shows how the coating process affects the characteristics of hydroxyapatite”, *Acta Biomater.*, **9** [12] (2013) 9538–9546.
  31. S. Saber-Samandari, K. Alamara, S. Saber-Samandari, “Calcium phosphate coatings: Morphology, microstructure and mechanical properties”, *Ceram. Int.*, **40** [1] (2014) 563–572.
  32. S. Saber-Samandari, K.A. Gross, “Micromechanical properties of single crystal hydroxyapatite by nanoindentation”, *Acta Biomater.*, **5** [6] (2009) 2206–2212.
  33. S. Saber-Samandari, K.A. Gross, “Amorphous calcium

- phosphate offers improved crack resistance: A design feature from nature?", *Acta Biomater.*, **7** [12] (2011) 4235–4241.
34. H.D.B. Jenkins, K.P. Thakur, "Reappraisal of thermochemical radii for complex ions", *J. Chem. Educ.*, **56** [9] (1979) 576–577.
  35. A. Fakharzadeh, R. Ebrahimi-Kahrizsangi, B. Nasiri-Tabrizi, W.J. Basirun, "Effect of dopant loading on the structural features of silver-doped hydroxyapatite obtained by mechanochemical method", *Ceram. Int.*, **43** [15] (2017) 12588–12598.
  36. P. Cheang, K.A. Khor, "Thermal spraying of hydroxyapatite (HA) coatings: effects of powder feedstock", *J. Mater. Process. Technol.*, **48** [1-4] (1995) 429–436.
  37. H. Li, K.A. Khor, P. Cheang, "Thermal sprayed hydroxyapatite splats: nanostructures, pore formation mechanisms and TEM characterization", *Biomaterials*, **25** [17] (2004) 3463–3471.
  38. P. Fauchais, "Understanding plasma spraying", *J. Phys. D. Appl. Phys.*, **37** [9] (2004) R86–R108.
  39. K.A. Gross, M. Babovic, "Influence of abrasion on the surface characteristics of thermally sprayed hydroxyapatite coatings", *Biomaterials*, **23** [24] (2002) 4731–4737.
  40. T.F. Page, S.V. Hainsworth, "Using nanoindentation techniques for the characterization of coated systems: a critique", *Surf. Coat. Technol.*, **61** [1-3] (1993) 201–208.
  41. B. Bhushan, X. Li, "Nanomechanical characterisation of solid surfaces and thin films", *Int. Mater. Rev.*, **48** [3] (2003) 125–164.
  42. L.P. Mullins, M.S. Bruzzi, P.E. McHugh, "Measurement of the microstructural fracture toughness of cortical bone using indentation fracture", *J. Biomech.*, **40** [14] (2007) 3285–3288.
  43. M. Marrese, V. Guarino, L. Ambrosio, "Atomic force microscopy: a powerful tool to address scaffold design in tissue engineering", *J. Funct. Biomater.*, **8** [1] (2017) 7.